Saudi Dental Journal (2019) **31**, 242–250

King Saud University

Saudi Dental Journal

www.ksu.edu.sa
www.sciencedirect.com

ORIGINAL ARTICLE

Implementation and characterization of coating pure titanium dental implant with sintered β-TCP by using Nd:YAG laser

Ihab Nabeel Safi [a], **Basima Mohammed Ali Hussein** [a,*], **Ahmed Majeed Al Shammari** [b], **Thaier Abid Tawfiq** [c]

[a] *College of Dentistry-University of Baghdad, Iraq*
[b] *Experimental Therapy Department, Iraqi Center for Cancer and Medical Genetic Research, Mustansiriyah University, Iraq*
[c] *Institute of Laser for Postgraduate Studies, University of Baghdad, Iraq*

Received 5 August 2018; revised 22 December 2018; accepted 26 December 2018
Available online 8 January 2019

Abstract *Objectives:* This work presents laser coating of grade 1 pure titanium (Ti) dental implant surface with sintered biological apatite beta-tricalcium phosphate (β-TCP), which has a chemical composition close to bone.

Materials and methods: Pulsed Nd:YAG laser of single pulse capability up to 70 J/10 ms and pulse peak power of 8 kW was used to implement the task. Laser pulse peak power, pulse duration, repetition rate and scanning speed were modulated to achieve the most homogenous, cohesive and highly adherent coat layer. Scanning electron microscopy (SEM), energy dispersive X-ray microscopy (EDX), optical microscopy and nanoindentation analyses were conducted to characterise and evaluate the microstructure, phases, modulus of elasticity of the coating layer and calcium-to-phosphate ratio and composition.

Results showed that the laser power and scanning speed influenced coating adherence. The cross-sectional field-emission scanning electron microscopy images at low power and high speed showed poor adherence and improved as the laser power increased to 2 kW. Decreasing the scanning speed to 0.2 mm/s at the same power of 2 kW increased adherence. EDX results of the substrate demonstrated that the chemical composition of the coat layer did not change after processing. Moreover, the maps revealed proper distribution of Ca and P with some agglomeration on the surface. The sharp peaks on the X-ray diffraction patterns indicated that β-TCPs in the coat layer were mostly

* Corresponding author.
E-mail address: basma.moh@ilps.uobaghdad.edu.iq (B.M.A. Hussein).
Peer review under responsibility of King Saud University.

Production and hosting by Elsevier

https://doi.org/10.1016/j.sdentj.2018.12.004

crystalline. The elastic modulus was low at the surface and increased gradually with depth to reach 19 GPa at 200 nm; this value was close to that of bone. The microhardness of the coated substrate increased by about 88%. The laser pulse energy of 8.3 J, pulse peak power of 2 kW, pulse duration of 4.3 min, repetition rate of 10 Hz and scanning speed of 0.2 ms^{-1} yielded the best results.

Conclusion: Both processing and coating have potential use for dental implant applications.

1. Introduction

Titanium and titanium alloys have been used widely for several decades as materials of choice for dental implants because of their biocompatibility, good mechanical properties, corrosion resistance, no cell toxicity and weak inflammatory response in peri-implant tissues (Gökmenoğlu et al., 2016). Positive modulation of biological processes is limited because it is unable to induce bone apposition (osteoinduction). Hydroxyapatite (HA) and β-tricalcium phosphate (β-TCP) were classified in sequence as bioactive materials on the basis of apatite formation (Avila et al., 2009). The bioactive coating calcium phosphate (CaP) is used to enhance osseointegration and improve the stability of dental implants. Since their use as bone grafts, CaP-based ceramics such as HA and β-TCP have received a great deal of attention because they are chemically and crystallographically similar to living bone; they are described as bioactive help in bone regeneration (Tian et al., 2005, 2006; Roy et al., 2008; Dorozhkin, 2013). Depending on its location, the CaP ratio in natural bone is 1.5–1.65, which is almost the same as the β-TCP ratio (Sieniawski and Ziaja, 2013). Regarding biodegradation, β-TCP has more advantages than α-TCP (Viswanath et al., 2008). Previous experiments showed that pure CaP coatings demonstrate weak bonding strength with substrates and exhibit poor stability (Jarcho, 1981; Hench, 1991; Liu et al., 2004; Mohseni et al., 2014). One obstacle to control bioactivity together with an excellent bonding strength of the coat without affecting the substrate properties as well as to prevent undesirable problems within living organisms happen from coat debris (Roy et al., 2008).

High coating crystallinity with good adherence, ability to control measurements and outline of the coating that covers the unique structures of a dental implant are important requirements for a successful coating. A favourable solution is the laser technique. Laser provides attractive surface modifications because it is unidirectional and has high coherence; both with other specific and unique laser criteria offer surface modification and treatment with high precision and specific area involvement without affecting the entire service area (Tian et al., 2005). Lasers are widely used as a coating technique to improve surface properties of several types of metals. Application of a CaP layer via laser coating enhances substrate performance during use (Ion, 2005; Jang et al., 2013). To obtain a desirable coating layer, powder is placed on the surface of a substrate with a binder or a molten pool is created on the surface of a substrate, which must be supplied with coat powder directly. In comparison with other coating techniques, laser coating helps to control and manage the size and shape of the coat layer or particles, as well as reduce the requirements or pre-surface preparation of the substrate (Comesaña et al., 2010).

The microstructure of melted HA powder on Ti via the laser technique is widely reported in the literature. Despite the good biological properties of β-TCP, few trials have been made to fabricate the β-TCP coat layer on commercially pure titanium grade 1 implant through surface treatments.

This paper reports the use of laser coating to fabricate a bioceramic layer on commercially pure titanium grade 1 at different laser parameters as a dental implant and evaluate the coating layer. Field emission scanning electron microscopy (FESEM), energy-dispersive X-ray spectroscopy (EDX), atomic force microscopy (AFM) and X-ray diffraction (XRD) analyses were conducted to examine the surface structure, Ca/P ratio and composition, surface roughness and phases. The elastic modulus (EM) of the coat layer and interfacial toughness were evaluated by using nanoindentation and Vickers hardness tests, respectively.

2. Materials and method

2.1. Sample and suspension preparation

Fifty specimens were prepared as circular discs of 2 mm in thickness and 6 mm in diameter by cutting commercially pure Ti grade 1 rods (Baoji Jinsheng Metal Material/China) with a water jet machine. These discs were ground and polished with SiC paper of 500, 800, 1200, 2000 and 2400 grit size; cleaned ultrasonically in absolute ethanol for 30 min and dried. About 100 ml of solution containing 92 ml of distilled water, 2 ml of hydrofluoric acid (HF) and 6 ml of nitric acid (HNO_3) was used as an etch solution for 3 min to remove the oxide film subsequently, the discs were rinsed with acetone before coating (AL-Sayed Ali et al., 2017). Approximately 0.3 g of β-TCP sintered powder (≥98% β phase basis, 49,963 Sigma–Aldrich) was dispersed in 10 ml of ethanol (≥99.8% GC 24,103 Sigma–Aldrich) to obtain a homogenous slurry, which was preplaced as a powder bed on the pure Ti surface; the substrate was spray-coated with the slurry (Azzawi et al., 2017; Cheng et al., 2005). The organic solvent (ethanol) was allowed to evaporate, and a thin layer of β-TCP powder was preplaced on the substrate.

2.2. Direct laser melting process

2.2.1. Laser coating procedure

Several trials were carried out to achieve suitable laser coating parameters for optimal coat layer adherence. A pulsed Nd:

YAG laser of 1064 nm wavelength (Han's Laser/China) was used with laser parameters including pulse peak power (P_p), pulse duration (t_P) and pulse repetition rate (PRR); Table 1 and Fig. 1. The most suitable laser parameters were chosen by examining the surface of the substrate using an optical microscope (Leica DM2500). The laser parameters were determined by the mathematical expressions associated with the pulsed laser as follows (Tzeng, 1999):

$$E = t_P \times P_P \quad (1)$$

$$E = PRT \times P_a \quad (2)$$

$$PRT = PRR^{-1} \quad (3)$$

where E is the pulse energy, t_P is the pulse duration, P_p is the peak power, P_{av} is the average power (W), PRT is the pulse repetition time (s), and PRR is the pulse repetition rate (Hz).

2.2.2. Final attempts of the coating process

Data collected from the pilot study showed that sample (D) with the laser parameters used were the best. Furthermore, the best coat layer was obtained by decreasing the scanning speed to 0.2 mm s^{-1}. This speed achieved an overlapping factor of 70%, as observed by the optical microscopy images. Final laser parameters and setup are shown in Table 2.

Each specimen was irradiated two times by the laser beam to form a coat layer. Firstly, the Ti surface was preheated, and melting was initiated. Secondly, the prepared β-TCP powder slurry was pre-placed over the preheated surface. The pre-placed coat layer was irradiated by the laser beam with the same work parameters for the second pass to achieve adherence. The specimens were fixed on a movable three-axis CNC table (software: Mach3Mill CNC controller) to control the scanning speed and were sliced into cross sections to examine (Taylor, 1998). The top surface and cross sections of the specimens were analysed by FESEM equipped with EDS.

2.3. Elastic modulus

Nanoindentation test was conducted to measure the Elastic modulus (EM) and nanohardness (NH) of β-TCP coat layer across the thickness of the specimen. The device was programed such that the diamond indenter tip (4 μm) was lowered until it touched the substrate and reached a depth of 450 nm. The applied load of 1000 μN was adjusted, and the velocity was 20 μm s^{-1} The ambient temperature was between 20 °C and 30 °C.

Table 1 Laser parameters.

Sample	Peak power (P_p) kW	Pulse duration (t_P) ms	Repetition rate Hz	Observations
A				As a control/Fig. 1A
B	1	3–10	1	No melting and just surface treating/Fig. 1B
C	2	3–10	1	No melting and a higher degree of surface treating/Fig. 1C
D	2	3–10	1–10	Surface melting/Fig. 1D
E	>2			Melting the whole thickness of the substrate/Fig. 1E

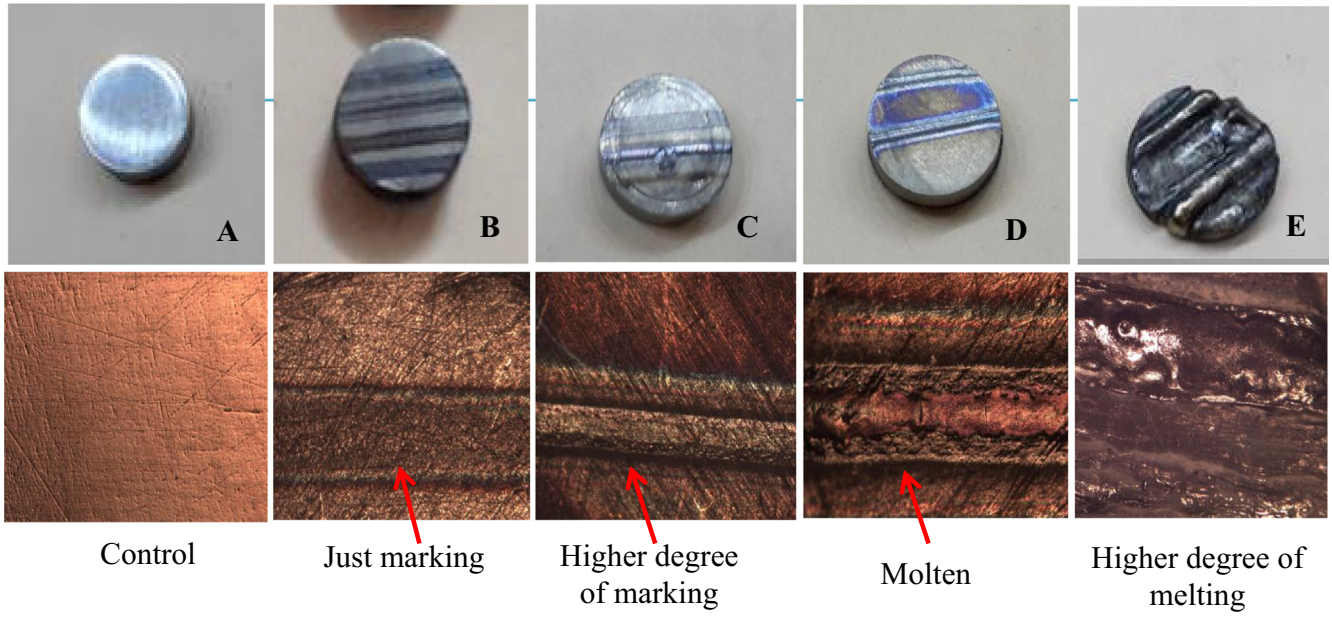

Fig. 1 Optical microscope images of the substrates' surfaces after different laser irradiating.

Table 2 Final laser parameters.

Parameters	Value
Laser power	2 kW
Standoff distance	8.6 mm
Beam width	0.5 mm
Line spot dimensions	6 * 0.5 mm
Scanning speed	0.2 mm s^{-1}
Repetition rate	10 Hz
Pulse duration	4.3 ms
Energy	8.30 J

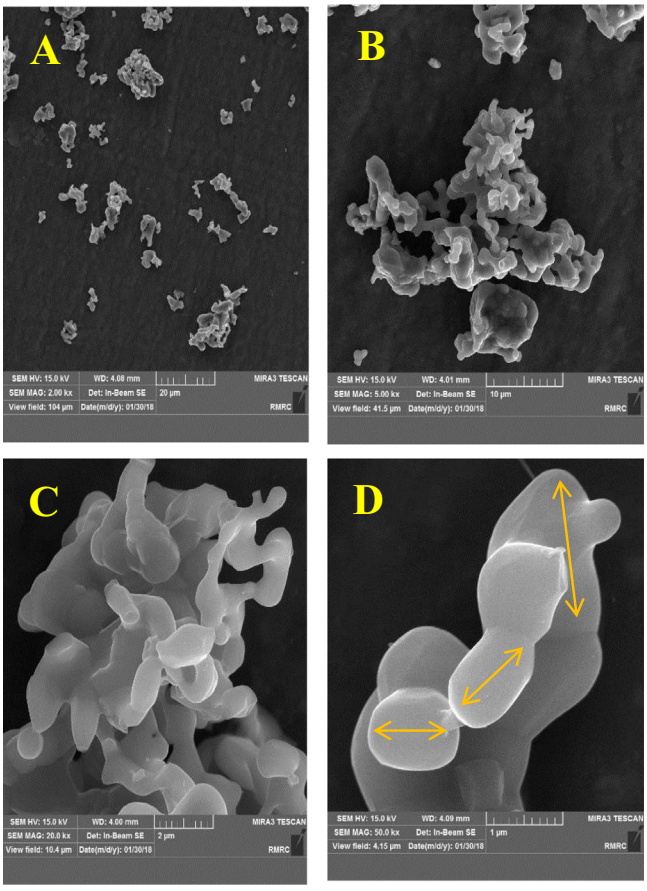

Fig. 2 FESEM micrographs of the sintered powder β-TCP (A. 2000X, B. 5000X, C. 20000X, D. 50000X).

2.4. Hardness of the coats

The microhardness of the coated substrates was measured by a Vickers micro-indentation tester in accordance with ASTM test standards E384-17 on a Buehler Micromet 5103. The microindentation applied force was 0.24 N along a period of 10–15 s at ambient temperature. An average of three readings was determined as the mean hardness value (HV).

3. Results and discussions

3.1. Particle size

To investigate the particle size of powder, FESEM type MIRA3 TESCAN was used. Particle size was ranging from 1 μm to 5 μm (Fig. 2).

3.2. Coat adherence

Both laser power and scanning speed influenced coat layer adherence. Low power laser and high scanning speed showed weak adherence and peeled off. Fig. 3 shows the cross-sectional micrographs of β-TCP coats, indicating variations in coating quality with the scanning speed. Coat layer adherence was improved when the laser power increased to 2 kW. When the scanning speed decreased from 1 to 0.5 and reached 0.2 mm s^{-1} at 2 kW, coat layer adherence increased. Melting pool depends on laser processing parameters; a reduction in scanning speed increases the depth, width and height of the coating by increasing the time for accumulation of heat on the surface of the substrate; as the melting pool increased, particles became entrapped inside the molten layer of Ti and forming a metallurgical bond (Shivamurthy, 2008).

3.3. Coat thickness and microstructure of interface

The cross-section FESEM images of the coated specimens showed that the average thickness of the coat layer was 13 μm (Fig. 4A). The interface of Ti-β-TCP, Fig. 4B indicates Ti surface melting, and β-TCP particles were completely and partially embedded with movement toward the coated surface (Fig. 4C). The high-resolution image in Fig. 4D shows good coating adhesion. Moreover, the interface between the coat

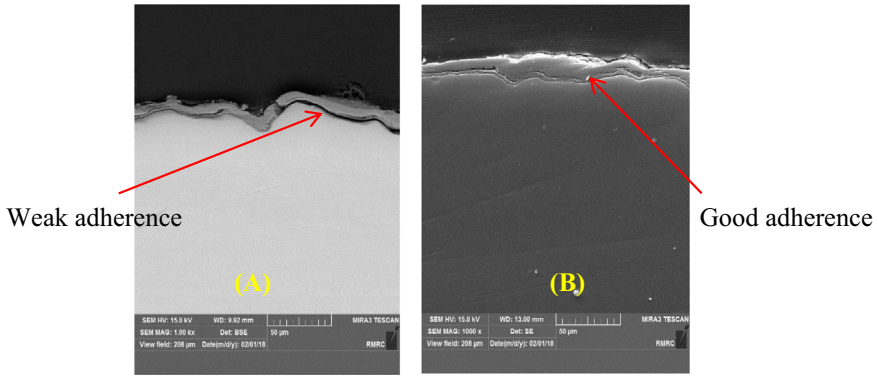

Fig. 3 FESEM cross-section images of the coat adherence as a function of 2 kW laser power and scan speed of; (A) 1 mm s^{-1}, (B) 0.2 mm s^{-1}.

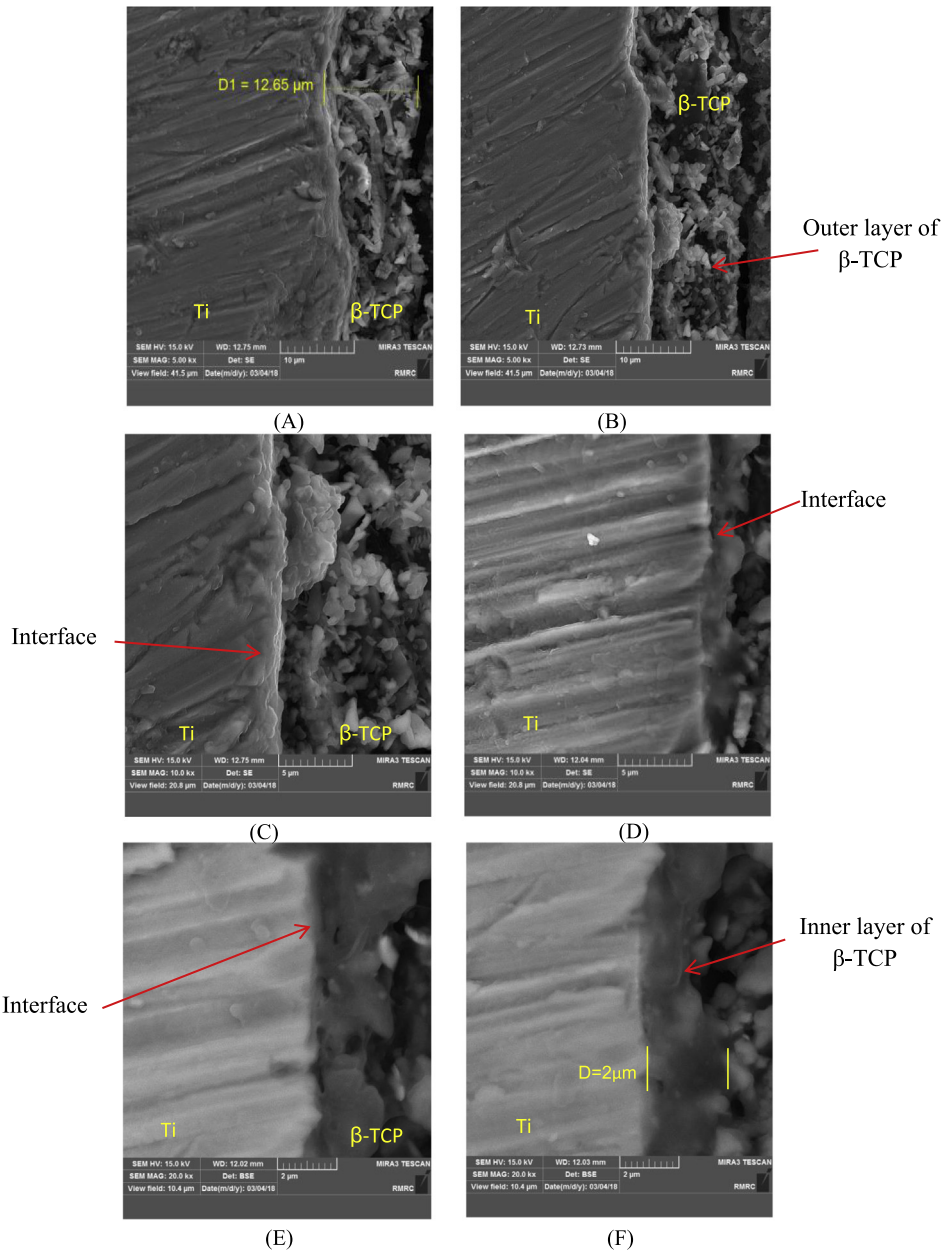

Fig. 4 FESEM cross-section images of β-TCP coat layer. (A and B) at 5000X, (C and D) at 10000X, and (E and F) at 20000X.

layer and the substrate was diffused due to the presence of β-TCP during solidification of Ti. The β-TCP particles were entrapped inside the molten layer of Ti, forming a metallurgical bond as indicated in Fig. 4E and F (Herman and Sampath, 1996; Cheng et al., 2005). In general, the coat layer is divided into two parts; thin and homogenous inner layer about 2 µm next to the substrate and an outer porous layer of about 10 µm, which represents β-TCP by the EDX spectra (Fig. 4B). The coat layer was softer at the surface and harder at the heat-affected zones. Fig. 4E and F show the cross section of the coat layer, which was a dense structure of 2 µm. The microporous outer layer was somewhat interconnected and did not penetrate through the inner layer towards the substrate. This phenomenon was mainly related to abundant particles deposited on the entire coat layer.

3.4. Surface microstructure

The surface topography of the uncoated substrate is illustrated in Fig. 5A. This figure also shows that the coat surface of β-TCP (Fig. 5B, C, and D) was continuous, crack-free, with uniformly distributed β-TCP particles and aggregates of different sizes. Furthermore, roughness of the coating surface was favourable because it help in bone tissue bonding, thereby improving osseointegration and enhancing prognosis. β-TCP particles were distributed in the coating layer.

3.5. Surface roughness

In this study, 3D roughness parameters (nm) were investigated via AFM. The mean values of five substrates were each tested

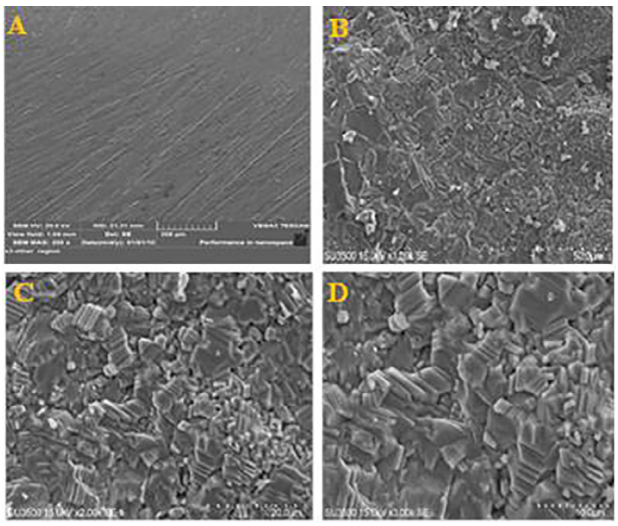

Fig. 5 SEM surface topographic image of (A) uncoated Ti. (B, C and D) SEM surface topographic images of coated substrate at different magnifications of 1000X, 2000X and 3000X.

at three different positions (Table 3). Such rough coating surfaces are advantageous because they enhance bonding to bone tissue in vivo (Eom et al., 2012; Rong et al., 2009). Applying bioactive ceramics and increasing roughness are the main causes to improve surface properties for titanium implants. The removal torque values directly related to rough implant surface aid in mechanical interlocking and improve the surface area (Chung et al., 2013).

3.6. Chemical composition

Chemical composition analyses of the coat layer was performed via SEM–EDS, and results confirmed the presence of β-TCP particles on the surface. The spectra contained Ca, Ti, P and O. The EDS spectra were used for elemental analysis on the surface and both Ca and P were well distributed within the coating (Fig. 6). The results of Fig. 6 are summarized in Table 4.

3.7. Ca/P ratio of β-TCP coating

The biocompatibility of β-TCP depends on chemical integrity, and the most important indicator of β-TCP is the molar ratio of Ca/P (Cheng et al., 2005). The β-TCP coating was chemically and crystallographically similar to natural bone; therefore, the coating simulated bone regeneration and reduce the time for osseointegration. The CaP film on the substrates during laser processing did not affect the Ca/P ratio. Table 4 shows the Ca/P ratio of the coating. The Ca/P ratio in the coat layer of 25.10/16.16 was 1.55, which was similar to the Ca/P ratio of 3/2 in $Ca_3(PO_4)_2$ given that the stoichiometric Ca/P ratio of β-TCP powder was 1.5. Thus, most of the constituent phase of the coat layer was β-TCP, which indicated that the

Table 3 Topographic analyses of the substrate surface roughness (nm).

Substrates	S_a (nm)	S_{dr} (%)	S_{dq} (/nm^2)	S_q (nm)
A. untreated Ti	13 ± 1	0.87 ± 0.06	0.133 ± 0.05	3.15 ± 0.3
B. treated Ti with laser	23 ± 1.3	5.76 ± 0.4	0.361 ± 0.06	7.08 ± 0.8
C. β-TCP coat	33 ± 2	9.26 ± 0.3	0.445 ± 0.07	9.37 ± 0.6

(±SD) S_a: roughness average, S_{dq}: slop root mean square, S_{dr}: increment of the interfacial surface area relative to a flat plane base line, Sq: height root mean square of the surface.

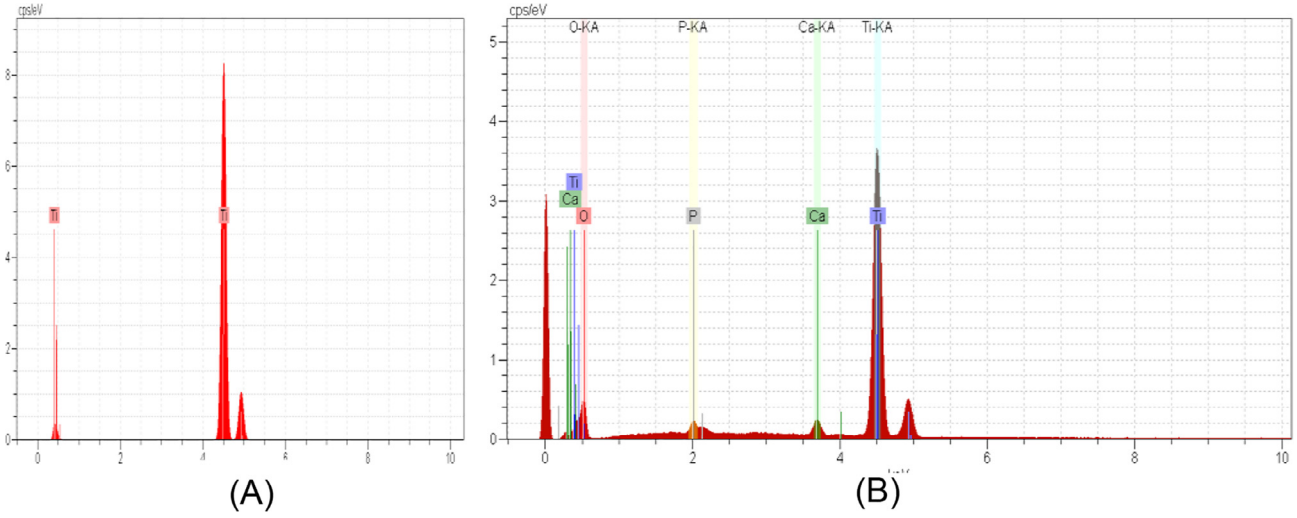

Fig. 6 EDX results of (A) control Ti surface substrate, (B) coated Ti substrate with β-TCP.

Table 4 EDX results of the coated substrate.

Element	Mass (%)	Atom (%)
Oxygen	37.02	57.51
Phosphorus	20.14	16.16
Calcium	40.48	25.10
Titanium	2.36	1.22

chemical composition of the coat layer was maintained after laser processing. β-TCP did not undergo thermal decomposition that may affect its biocompatibility. This effect was due to the transparency of β-TCP to infrared light, which allowed the Nd:YAG laser to penetrate the β-TCP powder and heat the Ti substrate whilst the β-TCP powders remained at low temperature. The rapid cooling rate and high specific heat of β-TCP allowed heat to be dissipated in the Ti substrate and air. The EDX maps showed the proper distribution of Ca and P particles with some agglomeration on the surface (Fig. 7).

3.8. Phase analysis

The phases of the coatings were characterized by XRD type Lab X 6000/SHIMADZU with a scan range of 10–80 and two thetas at 40 kV and 30 mA with a scanning speed of 8 u/min. Firstly, XRD patterns of titanium substrate and β-TCP were indexed to ICDD files (2012). The Ti substrate did not have any difference in phase after coating as shown in the evaluation level of XRD, which is an essential condition when treating Ti. The peaks at 100, 002, 101, 102 and 110 were similar without any significant change in the XRD spectra. However, alterations were observed in the peak intensity of 101, which was due to the induced strain on the substrate surface after processing (Choi et al., 2005). Moreover, TiO was detected due to the open environment under which the task was performed. Thus, Ti was readily reactive in open oxygen environments (Fig. 8A).

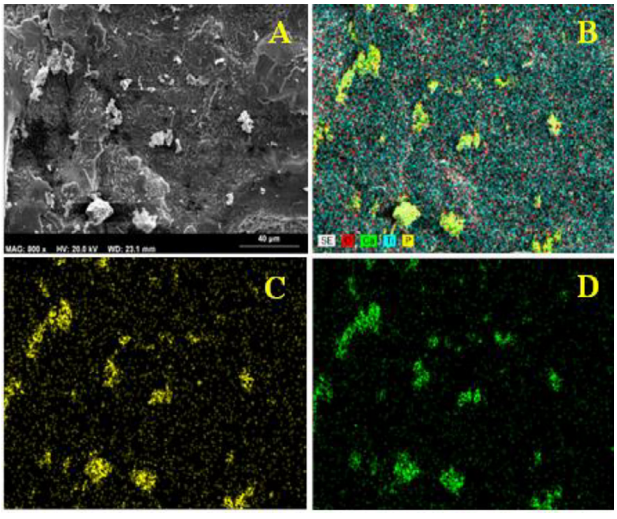

Fig. 7 SEM-EDS maps of coated Ti substrate surface. (A) Image of coated titanium, (B) distribution of Ti, O, P and Ca particles, (C) distribution of P particles, (D) distribution of Ca particles.

Ti substrates were treated by the laser beam before coating to enhance its roughness (Ciganovic et al., 2012) and then preheated to improve oxygen diffusion into the molten layer of the Ti substrate (Kalsoom et al., 2013). Both scenarios increased the surface adhesion properties.

The β-TCP coat layer has the same pattern of the ICDD standard 55-0898. The sharp peaks of the XRD patterns indicate that the β-TCPs in the coats are mostly crystalline as shown in Fig. 8B.

3.9. Mechanical properties

The elastic modulus (EM) and nanohardness (NH) of the β-TCP coat were measured at different depths of the β-TCP coat.

3.9.1. Elastic Modulus

EM was low near the top surface due to the pure and porous β-TCP coat and increased gradually with depth. At 1–10 nm, the EM was below 14 GPa. Meanwhile, the NH of the coat was constant at 7–18 GPa under 1–10 nm due to pure β-TCP ceramic coat.

At 10–200 nm depth, EM was found to be 19 GPa, which was close to the value of pure TCP ceramic (Wang et al., 2004) and natural bone (17–28 GPa of cortical bone and 0.5–3 GPa of cancellous bone). This low EM at the implant–bone interface is desirable for best stress distribution. As the depth increased to more than 200 nm towards the ceramic–metal interface, the EM increased due to the reinforced intermetallic compound phases (Cheng et al., 2005). Meanwhile, nanohardness decreased slightly with depth due to the intermetallic compound phases (Pichugin et al., 2008); Fig. 9.

The plot in Fig. 9 clearly indicates a brittle material such as HA due to the presence of elastic-plastic deformation. According to the Oliver–Pharr model (Yang et al., 2003), when dental implants are used, they must meet the requirements of both dentists and patients. Dentists prefer implant materials with high Young's moduli during operations, whereas patients need materials with low Young's moduli, approximate to that of bone (10–30 GPa), to help in proper stress shielding. Such properties reduce the chance for bone resorption and enhance bone remodelling (Niinomi et al., 2016). The strength of titanium should be increased while maintaining the low EM of the β-TCP coat.

3.9.2. Hardness of the coats

The hardness of the coated substrate was between 950 and 1150 VH (mean 1008.6 VH, SD ± 20.4) due to the use of sintered β-TCP powder as the coating material. This value was remarkably higher than that of the control, whose hardness was between 240 and 270 VH (mean 244.6, SD ± 43.3).

Therefore, the coat layer may not degrade or degrade very slowly over time. The slow degradation of the β-TCP coating occurred in the course of bone remodelling without loss of fixation, and osteoclasts probably played a major role. Degraded β-TCP at the interface likely induced the formation of new bone (Tanimoto and Nishiyama, 2008; Chien et al., 2009). Slow coating resorption and bone remodelling have resulted in an extent of bone-implant osseointegration.

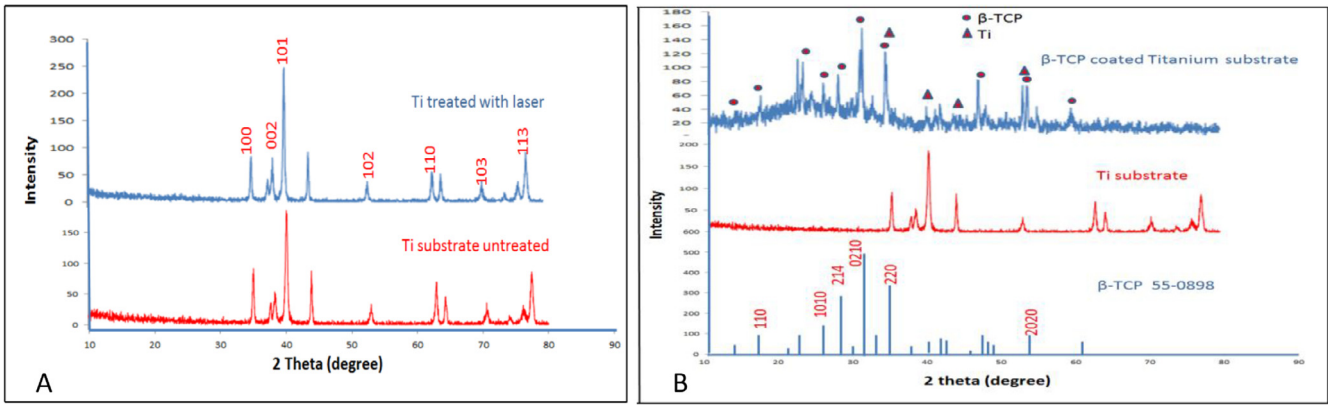

Fig. 8 (A) XRD pattern of untreated and treated Ti with 2 kW P_P and scanning speed of 0.2 mm s^{-1}, (B) XRD pattern of; β-TCP coat, titanium substrate and ICDD standard β-TCP 55-0898.

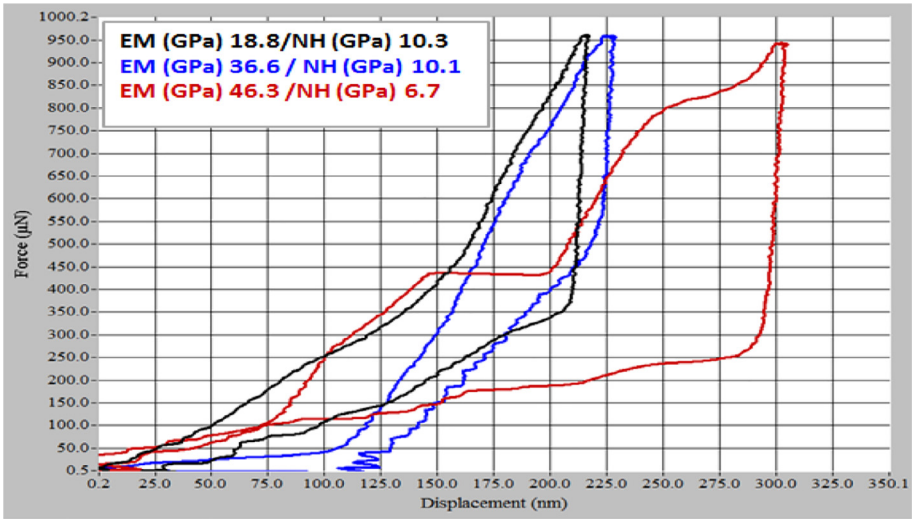

Fig. 9 The typical loading/unloading curves performed at the load of 1000 μN.

4. Conclusion

Unlike conventional deposition techniques, the laser melting technique can produce coatings with excellent mechanical properties and metallurgical bonding with high crystallites. This method can be used as a further modification procedure to enhance the β-TCP/titanium interface in dental implant applications.

Conflicts of interest

The authors declare they have no conflict of interests.

Ethical statement

(1) The manuscript is not currently being considered for publication in another journal;
(2) All authors have been personally and actively involved in substantive work leading to the manuscript, and will hold themselves jointly and individually responsible for its content.

References

Al-Sayed Ali, S.R., Hussein, A.H.A., Nofal, A.A.M.S., Hasseb Elnaby, S.E.I., Elgazzar, H.A., Sabour, H.A., 2017. Laser powder cladding of Ti-6Al-4V α/β Alloy. Materials 10, 1178.

Avila, G., Misch, K., Galindo-Moreno, P., Wang, H.L., 2009. Implant surface treatment using biomimetic agents. Implant Dentistry 18, 17–26.

Azzawi, Z.G.M., Hamad, T.I., Kadhim, S.A., 2017. A modified laser deposition technique for deposition titania nanoparticales on commercially pure titanium substrates. IJIRSET 6.

Cheng, G.J., Pirzada, D., Cai, M., Mohanty, P., Bandyopadhyay, A., 2005. Bioceramic coating of hydroxyapatite on titanium substrate with Nd-YAG laser. Mater. Sci. Eng. C 25, 541–547.

Chien, C.S., Han, T.J., Hong, T.F., Kuo, T.Y., Liao, T.Y., 2009. Effects of different hydroxyapatite binders on morphology, Ca/P ratio and hardness of Nd-YAG laser clad coatings. Mater. Trans. 50, 2852–2857.

Choi RJS, D., Steffier, W.S., Spearing, S.M., 2005. Residual stress in thick low-pressure chemical-vapor deposited polycrystalline SiC coatings on Si substrates. J. Appl. Phys. 97, 074904.

Chung, S.H., Kim, H.K., Shon, W.J., Park, Y.S., 2013. Peri-implant bone formations around (Ti, Zr)O(2) -coated zirconia implants

with different surface roughness. J. Clin. Periodontol. 40, 404–411.
Ciganovic, J., Stasic, J., Gakovic, B., Momcilovic, M., Milovanovic, D., Bokorov, M., et al, 2012. Surface modification of the titanium implant using TEA CO2 laser pulses in controllable gas atmospheres – comparative study. Appl. Surf. Sci. 258, 2741–2748.
Comesaña, R., Quintero, F., Lusquiños, F., Pascual, M.J., Boutinguiza, M., Durán, A., 2010. Laser cladding of bioactive glass coatings. Acta Biomater. 6, 953–961.
Dorozhkin, S.V., 2013. Calcium orthophosphates in dentistry. J. Mater. Sci. Mater. Med. 24, 1335–1363.
Eom, T.-G., Jeon, G.-R., Jeong, C.-M., Kim, Y.-K., Kim, S.-G., Cho, I.-H., et al, 2012. Experimental study of bone response to hydroxyapatite coating implants: bone-implant contact and removal torque test. Oral Surg. Oral Med. Oral Pathol. Oral Radiol. 114, 411–418.
Gökmenoğlu, C., Özmeric, Çakal, G., Dömetaş, N., Ergene, C., Kaftanoğlu, B., 2016. Coating of titanium implants with boron nitride by RF-magnetron sputtering. Bull. Mater. Sci. 39, 1363–1370.
Hench, L.L., 1991. Bioceramics: from concept to clinic. J. Am. Ceram. Soc. 74.
Herman, H., Sampath, S., 1996. In: Metallurgical and Ceramic Protective Coatings, pp. 261–289.
Ion, J.C., 2005. Laser processing of engineering materials: principles. Proc. Indus. Appl.
Jang, J.-H., Joo, B.-D., Van Tyne, C.J., Moon, Y.-H., 2013. Characterization of deposited layer fabricated by direct laser melting process. Met. Mater. Int. 19, 497–506.
Jarcho, M., 1981. Calcium phosphate ceramics as hard tissue prosthetics. Clin. Orthop. Relat. Res. 157, 259–278.
Kalsoom, U.-I., Bashir, S., Ali, N., 2013. SEM, AFM, EDX and XRD analysis of laser ablated Ti in nonreactive and reactive ambient environments. Surf. Coat. Technol. 235, 297–302.
Liu, X., Chu, P.K., Ding, C., 2004. Surface modification of titanium, titanium alloys, and related materials for biomedical applications. Mater. Sci. Eng. R: Rep. 47, 49–121.
Mohseni, E., Zalnezhad, E., Bushroa, A.R., 2014. Comparative investigation on the adhesion of hydroxyapatite coating on Ti–6Al–4V implant: a review paper. Int. J. Adhes. Adhes. 48, 238–257.
Niinomi, M., Liu, Y., Nakai, M., Liu, H., Li, H., 2016. Biomedical titanium alloys with Young's moduli close to that of cortical bone. Regener. Biomater. 3, 173–185.
Pichugin, V.F.S.R.A., Shesterikov, E.V., Ryabtseva, M.A., Eshenko, E.V., Tverdokhlebov, S.I., Prymak, O., Epple, M., 2008. The preparation of calcium phosphate coatings on titanium and nickel-titanium by rf-magnetron sputtered deposition: composition, structure and micromechanical properties. Surf. Coat. Technol. 202, 3913–3920.
Rong, M., Zhou, L., Gou, Z., Zhu, A., Zhou, D., 2009. The early osseointegration of the laser-treated and acid-etched dental implants surface: an experimental study in rabbits. J. Mater. Sci. Mater. Med. 20, 1721–1728.
Roy, M., Vamsi Krishna, B., Bandyopadhyay, A., Bose, S., 2008. Laser processing of bioactive tricalcium phosphate coating on titanium for load-bearing implants. Acta Biomater. 4, 324–333.
Shivamurthy, R.C., 2008. Effect of scanning speed, nozzle stand-off distance and beam scan-off distance on coating properties of laser surface alloyed 13Cr-4Ni steel. Trans. Indian Inst. Met. 61, 183–186.
Sieniawski, J., Ziaja, W., 2013. Titanium alloys -advances inproperties control. InTech.
Tanimoto, Y., Nishiyama, N., 2008. Preparation and physical properties of tricalcium phosphate laminates for bone-tissue engineering. J. Biomed. Mater. Res. Part A 85, 427–433.
Taylor, M.P., 1998. Assessment of plasma-sprayed hydroxyapatite coatings (Dissertation). Birmingham Univ.
Tian, Y.S., Chen, C.Z., Li, S.T., Huo, Q.H., 2005. Research progress on laser surface modification of titanium alloys. Appl. Surf. Sci. 242, 177–184.
Tian, Y.S., Chen, C.Z., Chen, L.X., Huo, Q.H., 2006. Microstructures and wear properties of composite coatings produced by laser alloying of Ti–6Al–4V with graphite and silicon mixed powders. Mater. Lett. 60, 109–113.
Tzeng, Y.F., 1999. Pulsed Nd:YAG laser seam welding of zinc-coated steel. Welding J. NY 78.
Viswanath, B., Raghavan, R., Gurao, N.P., Ramamurty, U., Ravishankar, N., 2008. Mechanical properties of tricalcium phosphate single crystals grown by molten salt synthesis. Acta Biomater. 4, 1448–1454.
Wang, C.X., Zhou, X., Wang, M., 2004. Influence of sintering temperatures on hardness and Young's modulus of tricalcium phosphate bioceramic by nanoindentation technique. Mater. Charact. 52, 301–307.
Yang, Y.C., Chang, E., Lee, S.Y., 2003. Mechanical properties and Young's modulus of plasma-sprayed hydroxyapatite coating on Ti substrate in simulated body fluid. J. Biomed. Mater. Res. Part A 67A, 886–899.